Published in final edited form as:
Macromolecules. 2010 December 14; 43(23): 9736–9746. doi:10.1021/ma101316w.

Curvature-coupled hydration of Semicrystalline Polymer Amphiphiles yields flexible Worm Micelles but favors rigid Vesicles: polycaprolactone-based block copolymers

Karthikan Rajagopal, **Abdullah Mahmud**, **David A. Christian**, **J. David Pajerowski**, **Andre E.X. Brown**, **Sharon M. Loverde**, and **Dennis E. Discher**
Chemical and Biomolecular Engineering, and Laboratory for Research on the Structure of Matter, University of Pennsylvania, Philadelphia PA 19104; Complex Assemblies of Soft Matter, Centre National de la Recherche Scientifique - Rhodia - University of Pennsylvania, Unité mixte internationale 3254, Bristol, Pennsylvania 19007, USA

Abstract

Crystallization processes are in general sensitive to detailed conditions, but our present understanding of underlying mechanisms is insufficient. A crystallizable chain within a diblock copolymer assembly is expected to couple curvature to crystallization and thereby impact rigidity as well as preferred morphology, but the effects on dispersed phases have remained unclear. The hydrophobic polymer polycaprolactone (PCL) is semi-crystalline in bulk (T_m = 60°C) and is shown here to generate *flexible* worm micelles or *rigid* vesicles in water from several dozen polyethyleneoxide-based diblocks (PEO-PCL). Despite the fact that `worms' have a mean curvature between that of vesicles and spherical micelles, `worms' are seen only within a narrow, process-dependent wedge of morphological phase space that is deep within the vesicle phase. Fluorescence imaging shows worms are predominantly in one of two states – either entirely flexible with dynamic thermal undulations or fully rigid; only a few worms appear rigid at room temperature ($T << T_m$), indicating suppression of crystallization by both curvature and PCL hydration. Worm rigidification, which depends on molecular weight, is also prevented by copolymerization of caprolactone with just 10% racemic lactide that otherwise has little impact on bulk crystallinity. In contrast to worms, vesicles of PEO-PCL are always rigid and typically leaky. Defects between crystallite domains induce dislocation-roughening with focal leakiness although select PEO-PCL – which classical surfactant arguments would predict make worms – yield vesicles that retain encapsulant and appear smooth, suggesting a gel or glassy state. Hydration in dispersion thus tends to selectively soften high curvature microphases.

Keywords

block copolymer; worm micelle; polymersome; crystallinity

Corresponding: discher@seas.upenn.edu.

Supporting Information. Molecular details of all polymers synthesized, calculation of polymer distribution in assemblies, AFM and fluorescence microscopy images, DLS and dye encapsulation studies, movies of worm micelles, persistence length measurement of worm micelles, procedure for measurement of contour lengths, and phase contrast images of OCL (2, 13.5) can be found in Supporting Information. Supporting Information is available free of charge on the internet at http://pubs.acs.org

Introduction

Amphiphilic block copolymers spontaneously self-assemble in water to form one of three basic morphologies – spherical micelles, worm-like micelles and vesicles (polymersomes).[1] Compared to supra-molecular assemblies derived from low molecular weight amphiphiles such as lipids and detergents, polymer-based assemblies possess a number of distinctive physical characteristics, including robustness.2 As a consequence of larger molecular weights, polymeric assemblies are thermodynamically more stable and sustain their morphologies longer after dilution. Polymer bilayers3, 4 and worm micelles[5, 6] can also be flexible even though they are thicker and less flexible than lipid counterparts. The choice of block chemistry and control of molecular weight allow for a reasoned manipulation of supra-molecular attributes such as shape, size, flexibility and stability. In applications such as drug delivery, flexible worm micelles function as long circulating carriers of hydrophobic drugs and dyes[7, 8] while polymersomes can effectively deliver – over a shorter duration – both hydrophobic and hydrophilic therapeutics.[9–11] In spite of the initial success, some block copolymers that are preferred for application are semi-crystalline in bulk, which raises basic questions about the interplay between crystallinity, hydration, and curvature.

Crystallization of organics – well beyond polymers – is of broad importance and is known to be highly sensitive to solution conditions. In bulk, crystallization of block copolymers favors lamellar phases, but crystallization can still be confined within spherical and cylindrical domains of strongly segregating blocks.[12] Dispersion of amphiphilic block copolymers in water might alter any intrinsic tendency to crystallize, since water generally permeates even the most hydrophobic cores – based on the observation that water will permeate a polymersome membrane (a singular lamellae) within seconds of establishing an osmolarity gradient across the membrane.[3] The prototype diblock copolymer for understanding hydration effects is perhaps polyethyleneoxide-*b*-poly(1,2-butadiene) (PEO-*b*-PBD, or OB), which is amorphous rather than crystalline and has been extensively studied as a function of molecular weight M and mass fraction of polyethyleneoxide block (f_{EO}).[13] As f_{EO} of the hydrophilic block is progressively decreased, spherical micelles give rise to worm micelles and then to bilayered polymersomes, thus generating the prototypical Sphere/Worm/Vesicle microphase behavior documented decades ago with small molecule surfactants.[14]

Polyethyleneoxide-*b*-polycaprolactone (PEO-*b*-PCL, or OCL) diblock copolymer is of interest here because PCL is semi-crystalline in bulk and because this biocompatible diblock is already being applied in drug delivery.[15–21] PCL is hydrophobic but hydrolytically degradable; and hydration of a PEO brush provides a kinetic barrier to protein adsorption, imparting `stealth' characteristics for these assemblies *in vivo*.[22] Worm micelles of OCL persist in the blood circulation and deliver more drug to tumors than spherical micelles[8] and while the effects of shape appear equally interesting with other polymer-based colloids,[23, 24] a deeper understanding is needed for the effects of PCL's crystallinity as it couples to micellar curvature, proximity to water, etc. Vesicles in addition to worm micelles can be made with OCL[25–27] and a branched derivative of PCL, PEO-*b*-poly(γ-methyl-ε-caprolactone), seems well-motivated by concerns over crystallization.[28] However, to broadly assess the effects of PCL's semi-crystalline nature on the phase behavior and properties of OCL dibock copolymers, we have synthesized a large set of polymers – including copolymers of PCL with racemic, biocompatible lactide (LA) in order to disrupt crystallization. We characterize individual worm micelles and vesicles by various dynamical micro-methods. We show that OCL strongly favors vesicle membranes over worm micelles compared to other amphiphilic block copolymers, and while some worm micelles are entirely rigid and all vesicles appear rigid, most worm micelles are highly flexible but stable to a limited range of process perturbations. A rugged energy landscape thus underlies the phases and rigidities of OCL assemblies.

Results and Discussion

Synthesis, bulk crystallization, and self-assembly in water

Ring opening polymerization of ε-caprolactone (CL) used stannous octoate as a standard catalyst and methoxy-PEO as the macro-initiator at 140°C to generate a series of 33 PEO-*b*-PCL diblock copolymers with four different sizes of PEO blocks. These are represented here as OCL(X, Y), where X and Y are the respective molecular weights of the two blocks in kg/mol. Since release of ring strain is the driving force for polymerization,[29] the synthesis also permits co-polymerization of a low concentration of racemic *DL*-lactide (LA) units within the PCL block (Scheme 1A). LA is hydrophobic, biocompatible and susceptible to hydrolytic degradation, in addition to being amorphous when polymerized, and the low concentration of LA favors a random polymerization despite reactivity differences.[30, 31] Two block copolymers incorporating 10 mol% LA within the PCL blocks were synthesized; polyethyleneoxide-*b*-poly(ε-caprolactone-*r*-*DL*-lactide), is denoted OCLA (X, Y, Z), where X (2 kg/mole) is the size of PEO and Y and Z are the respective masses of polymerized caprolactone and lactide. Polydispersity indices and block ratios for all of the synthesized polymers were respectively assessed using GPC and NMR spectroscopy as listed in Table 1 (and detailed in S1).

Semi-crystalline packing of PCL is shown in space-filling representation (Scheme 1B, left panel) based on a known crystal structure,[32] whereas packing within OCLA assemblies (Scheme 1B, middle panel) is predicted to be less ordered because LA's bulky methyl groups protrude and disrupt the crystal. Nonetheless, all of these polymers in anhydrous bulk form exhibit facets suggestive of massive crystallization (Scheme 1C), and differential scanning calorimetry demonstrates two transitions: a first small transition for PEO, the minor block, and a second larger transition for the pure or mixed polyesters (Scheme 1D). As expected, the second transition is suppressed in magnitude for OCLA (per gram), but it is also shifted to lower temperature as is the PEO transition. For comparison, OB is non-crystallizable copolymer that appears amorphous and exhibits only one calorimetric transition for PEO.

Aqueous phase self-assembly in dilute solution (≤100 μM) of OCLA and all OCL polymers was of principal interest and was initiated by several methods, including hydration of a chloroform solution of the polymer at room temperature with slow evaporation of chloroform. With gentle stirring to avoid fragmentation of growing assemblies, self-assembly was spontaneous and complete within 24–48 hours. Fluorescence microscopy images of various OCL morphologies were obtained by labeling with a lipophilic dye as shown in Figure 1A. Spherical micelles were typically visible only as `dots' of low fluorescence intensity (see S2), whereas worm micelles were unmistakable as elongated and flexible structures with some confirmed by AFM (see S3). Vesicles were clear as edge-bright assemblies and were verified when needed by encapsulation of fluorescein-labeled dextran (~4 kg/mol) within the aqueous lumen (see Figure 1A, inset). The relatively large size of the diblock copolymers (>1 kg/mol) results in the formation of stable and `giant' (> 1 μm) worm micelles and vesicles that allowed further physical characterization of their properties and dynamics using time-lapse fluorescence microscopy. Of principal interest is whether confined crystallization within high curvature geometries such as cylinder-shaped worm micelles impact structures and properties.

Morphological phase behavior

The preferred morphology of each block copolymer (see S4 for morphologies of all polymers) is mapped into a plot of core block hydrophobicity (M_{CH2}) versus hydrophilic mass fraction $f_{hydrophilic}$ (Figure 1B). These parameterizations differ slightly from past studies for polymers such as PEO-*b*-PBD (OB)[13] because the strength of segregation with

polybutadiene ($\chi_{PEO\text{-}b\text{-}PBD}$=0.336) considerably exceeds that of polycaprolactone ($\chi_{PEO\text{-}b\text{-}PCL}$=0.146) (see S5 for calculations). Group theory ideas suggest that the two oxygens per caprolactone monomer reduce PCL's hydrophobicity and contribute a degree of hydrophilicity, and so M_{CH2} and $f_{hydrophilic}$ are calculated by respectively subtracting or adding oxygen contributions from PCL. Such corrections shift the phase boundary between spherical micelles and the other morphologies to $f_{hydrophilic}$ ~ 0.5, which is remarkably similar to the same phase boundary for OB in terms of f_{EO}. The boundary here also shows only a weak shift in $f_{hydrophilic}$ from low to high molecular weight, which is also observed with OB diblocks.

Assembly is minimal for M_{CH2} < 1 kg/mol due to weak cohesive interactions, with a few micellar aggregates (Figure 1B, open triangles). At the 100 μM concentration used throughout, Dynamic Light Scattering (DLS) and fluorescent-dextran encapsulation studies show that while vesicles are made from OCL(1, 3), the smaller polymers OCL(1, 0.5) and OCL(1, 1) generate a few spherical micelles (low intensity) and micellar aggregates but no vesicles (see S6). Precipitation of polymer occurs when $f_{hydrophilic}$ < 0.36, presumably because short PEO chains cannot stabilize the assemblies (open circles). Surprisingly, between these intuitive boundary regions, the vesicle/worm/sphere phase behavior shows that worm micelles occur only within a narrow sub-phase deep in the vesicle region. Worm micelles made with either small molecule amphiphilies[14] or strongly segregating copolymers such as OB13 show worms to be an intermediate morphology between spherical micelles and vesicles – but not with OCL.

The two OCLA block copolymers studied here also generate worm micelles and, importantly, fit within OCL's worm micelle region after suitable parameterization. As elaborated below, the OCL and OCLA worm micelles are largely flexible whereas the OCL vesicles are rigid, and so curvature frustration of crystallization seems confined to just the small region of worm micelle formation. In other words, bilayered vesicles are favored as this leads to a parallel alignment of chains for cooperative crystallite growth (Scheme 1B).

Phase boundaries in Figure 1B (grey lines) are not sharp: coexistence of more than one type of morphology is clear in the transition regions, as also seen with OB.[13] Nonetheless, because dye:polymer ratios are kept constant, even a nanovesicle of diameter much smaller than optical resolution (Rayleigh criterion gives ~250 nm) can be readily distinguished from a spherical micelle based on fluorescence intensity differences (which scale as the square of the radius ratio; see S2 for calculations) and also based on Brownian motion differences (which decrease linearly with the radius ratio). In other words, a 50 nm vesicle will diffuse slower and appear 10-fold brighter than a 20 nm sphere micelle. Worm micelles generally coexist with vesicles, consistent with embedding of this phase within a vesicle phase. However, even for strongly segregating OB copolymers, coexistence regions were very large, appearing several-fold broader than the narrow sliver of worm micelle formation (f_{EO} ~0.5 to 0.55).

Assemblies of OB – with its amorphous and flexible PBD block – have been described as non-ergodic[12], which is also of concern with glassy polymers such as PS-*b*-PEO33, and process-dependent assembly appears intrinsic to compartmentalized micelles obtained with trifunctional block copolymers.[34] The morphological phase space of OCL diblocks described above might therefore only approximate the energetically preferred, equilibrium phase behavior, and so we further investigated the evolution of morphologies as a function of temperature and process with a set of three diblocks of varying core chemistries (OCL(2, 9), OCLA(2, 7.4, 1.6), OB(4, 6)). As shown in Figure 2, changing from good solvent (chloroform) to bad solvent (water) by evaporation of the chloroform (Method-1) gave for all three polymers worm micelles at 25°C and vesicles at 60°C. However, at 4°C while

OCL(2, 9) forms mostly vesicles that would be favored by planar crystallites, and OCLA(2, 7.4, 1.6) forms some worm micelles plus vesicles, OB(4,6) forms predominantly worm micelles. In a second standard method, we re-hydrated dried copolymer (Method-2): we started with a thin film of polymer cast on the surface of a glass vial – templating a lamellar phase most likely – and then water was added at various temperatures. At 60°C, OCL(2, 9) forms worm-like `Y' junctions, OCLA(2, 7.4 1.6) forms both vesicles and vesicles with attached worm micelles (`squids'), and OB(4, 6) forms a mixture of worm networks and vesicles. At 25°C, however, OCL and OCLA polymers did not assemble, even after two weeks, whereas OB generated worm micelles overnight. Thermal activation (or solvent fluidization in Method-1) seems required to melt the PCL, even if copolymerized as OCLA, consistent with the calorimetry studies (Scheme 1D). Nonetheless, either wormlike assemblies or vesicles form when assembly does occur for all three copolymers, including the OB diblock, which underscores the proximity in free energies of formation for these two meso-scale morphologies.

Curvature-suppressed Crystallization yields mostly Flexible Worms

Morphologies described above are mere snapshots of more informative dynamics. Fluorescent movies of OCL worm micelles in water clearly show that most of these microns-long assemblies undergo incessant transverse fluctuations along their contour (see S7 for movie). This Brownian motion of flexible cylinders suggests a soft, fluid core. In contrast, a small but striking population of OCL(2, 9) worm micelles appears completely rigid along the entire contour length (see S7 for movie), rotating and translating as rigid rods (Figure 3A, top row panels). For OCLA, and also OB, there were no rigid worm micelles (Figure 3A; see S8 and S9 for movies). The all or none nature of flexibility versus rigidity indicates, of course, a two state process of crystallization.

The percentage of rigid worm micelles, θ, in a sample should in principle depend on molecular weight and temperature. Direct counting gives θ as a function of the size of hydrophobic block (M_{CH2}) for a series of OCL(2,Y) polymers (Figure 3B). The complete absence of rigid worm micelles in both OB and OCLA samples is also indicated. The molecular weight dependent results for the OCL(2,Y) series were fit ($R^2 = 0.985$) to a percolation-type power law

$$\theta(M_{CH2} - M_A)^{\gamma} \quad \text{Eq. 1}$$

in which M_A (≈ 4.284 kg/mol) is a critical molecular weight for nucleation of the hydrophobic block in rigidity percolation, and γ (≈ 0.68) is the percolation exponent. The most direct evidence for a critical molecular weight is provided by the polymer OCL (2, 6) which exhibits a vanishing small fraction of rigid worm micelles (0.5% ±0.15%) and has M_{CH2} ≈ 4.4 kg/mol that is only slightly higher than M_A. As suggested below, γ should increase with decreasing temperature. Rigidity percolation has been quantified previously in both worm micelles and vesicle membranes with blends of crosslinkable OB and the hydrogenated, non-crosslinkable form of the same copolymer. For worm micelles[4], γ ≈ 1 and for membranes[35], γ ≈ 1.5, which fit a general form previously noted in the latter studies:

$$\gamma = (D+1)/2 \quad \text{Eq. 2}$$

in which *D* is the dimensionality of the aggregate, i.e. *D* = 0, 1, 2 for spheres, worms, and membranes, respectively. For the crystallization here, γ ≈ 0.68 implies a (T-dependent) dimensionality between spheres and worms of *D* ≈ 0.2 for the fractal dimension (at T =

25°C) of the nucleating crystal that determines all-or-none rigidification of OCL worm micelles.

In addition to the rigidity scaling, the fit in Figure 3B suggests crystallization within a cylinder morphology is `frustrated' when the size of the hydrophobic block (M_{CH2}) is much less than ~4.3 kg/mole (M_A). Crystal formation occurs as a result of chain folding and close packing (Scheme 1B), and since core diameter of fluid worm micelles scales with core molecular weight[13] as $d \sim M^{0.67}$, the core curvature ($1/d$) is more suppressive at low molecular weight than at high molecular weight. A tightly confining curvature within the nanoscale cylindrical core of worm micelles is also likely to introduce many defects that limit crystallization, which is consistent with just 10% amorphous *DL*-lactide structurally limiting core-crystallization in OCLA worms.

With decreasing temperature, θ increases (Figure 3C; written as a fraction rather percentage). A majority of worm micelles are rigid at large under-coolings (θ = 0.6 at T = −20°C), and the proportion of rigid worm micelles nearly vanishes as T approaches bulk T_m (θ < 0.05 at T = T_m = 60°C). While this clearly indicates PCL crystallization in the worm micelle core as the mechanism driving rigidification, the transition is considerably broadened and shifted to lower temperature with curvature at the nano-scale: T ≈ −16°C appears to be the temperature for an equal probability of being crystalline or not. Melting point suppression that increases here with the curvature of worm micelles is shown below to be minimal with bilayer vesicles.

From hours to week(s) after formation, rigid worms remain a similar fraction of total worms in a sample, suggesting stability and perhaps equilibration. Temperature jumps (4°C → 60°C and 60°C → 25°C, not shown) likewise fall on the same basic curve, suggesting thermodynamic states. As an all or none process within each worm micelle, we therefore fit the data in Fig.3C to a two state model ($R^2 = 0.98$)

$$\theta = exp\left(-\Delta G/k_B T\right) / \left[N + exp\left(-\Delta G/k_B T\right)\right] \quad \text{Eq. 3}$$

in which ΔG is the free energy difference per giant worm micelle between crystalline and melted states and N is the effective number of distinct melted state configurations that oppose the low entropy crystalline state. The free energy difference of $-13.5\ k_BT$ (for T ≈ 300 K) is typical of macromolecular associations such as crystallization. The best fit $N \sim 6\times10^6$ is more difficult to understand, but each PCL chain of OCL(2, 9) has about n ~ 100 monomer units that undergo a random walk while entangled with dozens of other chains within any given cross-sectional slice of a worm micelle, and so the number of states multiply quickly.

Half-rigid worms of OCL were also seen (Figure 4), but these were a small sub-population of the rigid worms that decreased in number over days. As rare and transient intermediates, their existence is consistent with nucleation-growth of crystals that propagate within the core, along the worm contour. The rigid segments are generally straight over microns and then sometimes kinked or at least slightly curved. Given an estimated interfacial area per copolymer of ~1 nm × 1 nm[36], the rigid segments involve crystallization of 1000's of molecules before a collective defect frustrates further, rapid crystal growth. With time, however, such defects seem to anneal away to yield fully rigid worms.

Persistence length of worm micelles

The flexibility of most OCL worms and all OCLA worms is evident in the changing conformations and can be quantified in terms of the mean end-to-end distance (R). At short

time intervals (~ 50 msec), transverse fluctuations occur homogeneously along the contour length, consistent with a lack of any local rigidification. The persistence length (l_p) – if standard models fit – provides a measure of bending rigidity with a higher persistence length indicating a stiffer worm that is harder to bend. Imaging of fluorescently labeled worm micelles was done after confinement within a ~micron-gap between a glass slide and a cover slip, leading to quasi-2-dimensional ensemble of conformations. At 4-second intervals, conformations appear fully de-correlated, and from time-lapse images the end-to-end distance (R) and contour length (L) are readily measured (Figure 5A - inset). Using the mean square end-to-end distance ($<R^2>$) and the contour length (L), we find excellent fits of the data (Figure 5A) to a worm-like chain model (Kratky-Porod model)[37] given as

$$<R^2>=2(l_p)^2\left[(L/l_p)\right]-1+exp\left(-L/l_p\right) \quad \text{Eq. 4}$$

For OCL(2, 9), OCLA(2, 7.4, 1.6) and OB(4, 6) worm micelles made from copolymers of similar total molecular weight (M_{tot} ~ 11, 10), respective persistence lengths are 4.3 ± 0.44 μm (R^2= 0.95), 3.73 ± 0.34 μm (R^2=0.95) and 7.2 ± 0.5 μm (R^2=0.98), which indicates roughly similar physics. We verified that the dye is minimally perturbing to the worm dynamics by varying the dye to polymer ratio from 0.001 to 0.1 with no perceptible change in persistence length (see S10).

Bending of almost any type of long cylinder is expected to depend on diameter, and since worm diameter scales with molecular weight, the dependence of l_p on M_{tot} was examined for OCL (see S11 for l_p of OCL(2, 6) and OCL(2, 9)) as done previously for OB worm micelles.[6] Figure 5B suggests that both datasets for visibly stable giant worm micelles (with contour lengths $L > l_p$) fit to a percolation type model:

$$l_p=B(M_{Tot}-M_B)^{\delta} \quad \text{Eq. 5}$$

where B is a pre-factor, M_B is a critical molecular weight of the diblock at which l_p vanishes, and δ is the scaling exponent. A non-zero value for M_B is perhaps not intuitive, but we believe that it captures the idea that for $M_{Tot} < M_B$ thermally driven transverse fluctuations dominate and physically disrupt giant worm micelles. There is an implicit notion of *persistence in time* for a rigidity such as a persistence length; if molecules exchange with bulk and reside in an assembly on a time scale (~1/CMC) less than that of large collective fluctuations of the assembly (eg. bending), then a rigidity such as a persistence length would seem undermined. To our knowledge, there are no reports (no movies, especially) of giant worm micelles formed from very low molecular weight surfactants, and similar comments apply to giant vesicles. To be specific with lipid vesicles, two phosphatidylcholine-type lipids with either two 13-carbon chains or two 22-carbon chains (1.7-fold difference) have been shown to yield vesicles with the same surface elasticity (i.e. same interfacial tension) but respective bending moduli of 14 k_BT or 30 k_BT (2.1-fold) and respective rupture tensions of ~3 mN/m or >12 mN/m (>4-fold at stress rates); the lower value is so small that shorter lipids do not even generate giant vesicles that can be studied.[38] Such non-trivial scaling with molecular weight (see S12 for fitting Eq.5 to lipid results) is typical of soft matter assemblies: normal modes scale with system size and ~k_BT of thermal excitation per collective mode seems sufficiently violent that assemblies cannot be sustained on long length scales unless cohesion is sufficient, and of course cohesive stability against rupture increases strongly with molecular weight of amphiphile whereas interfacial tension *does not*. A `vanishing' persistence length of giant worm micelles in Eq.5 thus implies that at molecular weights below a critical value (scaling alternatively with [d −

d_o] in the work of Evans and coworkers[38], thermal undulations of worms tend to alter morphology (perhaps to spheres or vesicles) without significant effects on the intrinsic interfacial tension.

For OB worms, we find M_B = 4800 g/mole which seems a surprisingly large critical molecular weight. Since no OCL worms could be observed at M_{tot} < 6000 g/mole (Figure 1B), we assume for convenience that M_B = 4800 g/mole (expected to be higher) to obtain δ_{OCL} = 0.85 (R^2 = 0.94), which is slightly higher than δ_{OB} = 0.58 but then the pre-factor for OB is ~200-fold higher. No theory has yet predicted the critical scaling form of Eq. 5, and so the relationship of B or δ to parameters such as χ is yet to be established.

Contour length distributions of OCL worm micelles

Theories are available for length distributions $f(L)$ of worm micelle contour length, and include a one-dimensional self assembly model[14] and a Zimm-Shulz model[39] $f = b\, L \exp(L/L_n)$ in which b is a pre-factor and L_n is the number average contour length. In order to quantitatively estimate the distribution in countour lengths, worm micelles were immobilized and straightened on the surface of a glass coverslip, which could be achieved by adjusting the salt concentration. Images were digitally processed for several hundred worm micelles per sample to obtain the normalized contour length distributions for four worm-forming OCL diblock copolymers (Figure 6A) (see S13 for detailed procedure). The Zimm-Shulz model fit (R^2 > 0.99 for all four fits) helps to highlight the fact that as the size of the PCL block is increased, the proportion of longer worms increases while the proportion of shorter worms decreases. The bottom panel shows the increase in the proportion of worm micelles longer than 5 μm (P_{long}) as well as the experimentally determined average contour length (<L> which relates to L_n) as a function of the size of the hydrophobic block (M_{CH2}). The simplest one-dimensional self assembly model[13] predicts, as found, a linear relationship between L_n and M_{CH2}: longer hydrophobic chains increase cohesive (hydrophobic) interactions as χN.

The chemical metric of stability of amphiphilic assemblies is the critical micelle concentration or CMC, with simple models predicting CMC ~ exp(−χN); concentrations above this should generate increasingly longer worms.[39] For OCL(2, 9) from c = 0.011 to 1.1 mg/mL, the worm length distributions were fit to the Zimm-Schulz model (Figure 6B – upper panel, R^2 > 0.97 for all fits), and both the number average length (L_n) and the experimentally estimated average length (<L>) plotted as a function of polymer concentration (Figure 6B – lower panel). Scaling to ~c^{α} yields small exponents of α ~ 0.06, whereas one-dimensional self-assembly[14] predicts a much stronger dependence of α ~ 0.5, which indicates a substantial deviation from classical mean-field behavior. Winnik and co-workers[39] observed similar deviation in the formation of cylinders from crystalline polyferrocenyldimethylsilane-based diblock copolymers.

Vesicles of OCL and their physical characterization

Unlike worm micelles, vesicles are formed within a broader region of morphological space (Figure 1B). While most of the vesicles formed by chloroform evaporation method are less than 5 μm in size, film re-hydration at 60°C yields larger vesicles. Phase contrast images of OCL(2, 13.5) vesicles appear smooth and rounded at 60°C (Figure 7A), and vesicles made in a solution of 300mOsm sucrose and then visualized in glucose also appeared phase dark due to the refractive difference between outer solution and the retained inner solution. Upon cooling to 25°C, however, the vesicles not only appeared rough and irregular in shape but also lost the phase dark contrast. Cracks or holes that increase membrane permeability has been seen before with vesicles made from lipids that undergo phase transitions.40 Membrane roughening has also been associated with dislocation defects in flexible

membranes with crystalline order.[41] Vesicles made with non-crystalline OB(3.5, 6.75) always appear smooth and do not lose phase contrast upon cooling. At the intermediate temperature of 40°C, the OCL vesicles appear smooth but most have lost their phase contrast (Figure 7B); the temperature that yields 50% phase dark OCL vesicles is ~50°C. This temperature seems consistent with Scheme 1D's result for bulk OCL copolymer which exhibits a crystal to fluid transition of the PCL block upon heating above ~50°C. For worm micelles, 50% rigid worms were seen at ~0°C (Figure 3C), with the difference between vesicles and worms highlighting the curvature-suppression of the crystallization transition.

Rigidity of the polymer membranes was probed directly by aspiration into glass micropipettes (~2–4 μm diameter) using controlled pressures. For OCL(2, 13.5) vesicles at 25°C, even an applied pressure of 20 kPa did not induce any membrane deformation (Figure 7C) for any vesicle (n = 10 vesicles), consistent with a crystalline nature to the PCL within the bilayer core. In a few cases, as the pressure was increased further, the vesicles ruptured abruptly, indicative of cracking of the crystalline bilayer (S14). In contrast, aspiration of an OB(3,5, 6.75) vesicle membrane (Figure 7C) shows fluid-like deformation at minimal pressures (~1.3 kPa) with large distension of membrane at higher pressures (20 kPa).

An important exception to the OCL vesicle responses described above is seen with the copolymer OCL(2, 6), which has a composition that places it uniquely in the morphological phase diagram (Figure 1B) between the worm and sphere micelle phases. Crystallization of PCL favors the flat bilayer here, but OCL(2, 6) still seems to have some flexibility – like OCL worms – because vesicles of OCL(2, 6) do not crack and leak upon cooling (Figure 7A). Direct mechanical tests of nonetheless suggest membrane rigidity as well as a tendency to rupture at low pressures (Figure 7C). This is consistent with rigidity percolation seen in worms from the same copolymer (Fig. 3B, Eq. 1), and the membrane features here likewise suggest gel or glassy state membranes.

A free energy landscape of OCL Worm Micelles and Vesicles

In a final set of experiments, the thermal stability of worm micelles as a function of temperature was assessed for OCL(2, 9) polymer. A sample of OCL(2, 9) worm micelles was prepared by chloroform evaporation at 25°C and then either cooled to 4°C or heated to 60°C (Figure 8A). After equilibration for a day, both processes decreased the population of worms, whereas a sample of OB(4, 6) showed no such change in morphology as a result of heating or cooling (see S15). At low temperatures, enhanced crystallization of PCL stabilizes vesicles over worms. Transformations of worms to vesicles can be difficult to document: if one-hundred 8 μm long worm micelles (which fill a field of view) transform to vesicles upon cooling, then only a single 2 μm diameter rigid vesicle would be generated (see S2). At high temperatures, a possible decrease in χ_{OCL} and increased thermal fluctuations promote disassembly of worms to spheres and possibly more vesicles.

The thermodynamics of semi-crystalline assemblies are represented schematically by the free energy landscape of Figure 8B. The X-axis represents the curvature of the different morphologies, and the widths of the free energy valleys indicate the flexibility of each system. Since worm micelles co-exist with vesicles, these morphologies have nearly identical free energy minima, i.e. identical chemical potentials per chain. The underlying energetics of semi-crystalline morphologies in dilution depend strongly on the block ratios and temperature as well as the history of the self-assembly process.

Conclusions

Self-assembly in water of a large set of semi-crystalline PEO-*b*-PCL diblock copolymers modifies the standard Vesicle/Worm/Sphere phase behavior as crystallization couples to

curvature and hydration. With worm micelles, PCL crystallization seems evident only at very low temperatures and with high molecular weights. Core crystallization is typically manifested in the formation of rigid assemblies and favors low-curvature vesicles. For applications such as delivery of entrapped drugs or flow through the vasculature, the presence of rigid and/or leaky assemblies, even in small numbers will limit functionality. The results here show clearly that rigidity is unavoidable with pure PCL but can be eliminated by incorporating 10% *DL*-lactide within the PCL block.

Experimental Section

Synthesis of PEO-*b*-PCL (OCL) and PEO-*b*-P(CL-*r*-*DL*-LA) (OCLA) diblock copolymers

All PEO-*b*-PCL block copolymers were synthesized by the ring opening polymerization of ε-caprolactone using the required size of methoxy terminated polyethyleneoxide as macro initiator and stannous octoate as catalyst (see Scheme 1a). Briefly, freshly distilled ε-caprolactone (2.5g, 0.0219 moles), required amount of methoxy-PEO (amount based on required MW of block copolymer), and stannous octoate (15 mg, 3.7×10^{-5} moles) were weighed out in a flamed and nitrogen-dried ampule. The ampule was sealed and placed in an oven pre-equilibrated to 140°C and the polymerization reaction was allowed to proceed for 4 hours. The reaction was terminated after cooling the ampule to room temperature. For the synthesis of OCLA (2, X, Y) copolymers, a mixture ε-caprolactone and *DL*-lactide were taken along with required amount of polyethyleneoxide (2000 g/mole) and stannous octoate.

Estimation of block ratios by NMR spectroscopy

The synthesis of polymers was verified from NMR spectra collected using a Bruker NMR360 spectrometer. The block ratios were calculated from the integrals at 3.6 ppm (methylene protons of PEO) and 4.05 ppm (methylene protons of caprolactone).

GPC analysis

The molecular weight distributions of all the synthesized polymers were determined by gel permeation chromatography using a Waters system equipped with a Waters 1215 binary pump and Waters 2414 refractive-index detector. Separation was performed using Styragel HR2 column, calibrated with polystyrene standards and tetrahydrofuran as solvent.

Preparation of polymer assemblies

Polymer assemblies were prepared using two different methods. In the solvent evaporation method, a 1 mM stock of the polymer was first prepared in chloroform. 100 μL of this stock was then added to 1 mL of DI water taken in a clean 2 mL glass vial. The contents of the vial were stirred gently (~ 200 rpm) on a magnetic stir plate using a micro-stirrer with the cap open at room temperature. Stirring was continued for 48 hours or until no chloroform layer was observed. The final polymer concentration after chloroform evaporation was 100 μM. For solvent evaporation method at 4°C, the vial was stirred with cap open in a cold room (at 4°C) for 4 to 5 days or until no chloroform layer was observed. For solvent evaporation at 60°C, the vial was stirred with cap closed for 24 hrs or until chloroform has evaporated. For sample preparation using the film re-hydration method, 100 μL of 1 mM polymer stock solution is diluted to 800 μL with chloroform in a 4 mL glass vial. Chloroform was evaporated by gently purging nitrogen into the vial until a thin film of the polymer was formed on the inner surface and the vial was further dried in vacuum for at least 8 hours. To the dried vial, 1 mL of DI water was added and vial was placed in a pre-heated oven at 60 °C with cap closed and gently stirred (~100 rpm) for 12 hrs.

Flourescence microscopy imaging

100 μL of 100 μM polymer solution was taken in an eppendorf tube and 0.2 μL of 0.2 mM fluorescent dye (PKH26, Sigma) was added and gently mixed. From this, 2 μL of the sample was spotted on a pre-cleaned cover glass slide and an 18 mm circular cover slip was placed on top, pressed gently and sealed with vacuum grease on the sides. The cover slip was imaged using 60× lens with oil at 1.5× magnification on Olympus IX71 microscope equipped with a Cascade 512B camera. In order to visualize giant vesicles, 15 μL of this sample was taken in a thin chamber formed between a cover slip and glass slide using vacuum grease.

Measurement of percentage of rigid worms

100 μL of 100 μM polymer solution was taken in an eppendorf tube and equilibrated at the required temperature (4°C or 60°C) for a day. For imaging 0.2 μL of 0.2 mM dye (PKH26, Sigma) was added and gently mixed. 2 μL of this sample was spotted on a clear glass slide and a 18 MM cover slip is placed on top, pressed gently and sealed with grease. Imaging was done on Olympus IX71 microscope equipped with a Cascade 512B camera. For each sample 200 worm micelles were randomly counted from 10 different fields of view and the number of rigid worm micelles were recorded.

Estimation of worm micelle persistence length (l_p)

To 100 μL of 100 μM worm micelle solution, 0.2 μL of dye (0.2 mM PKH26, Sigma) was added. From this, 10 μL was removed and diluted to 100 μL with DI water. 2 μL of this was spotted on a pre-cleaned glass cover slide and 18 mm circular cover slip is placed on top, pressed gently and sealed with grease. The cover slip was imaged on Olympus IX71 microscope equipped with a Cascade 512B camera. Five time-lapse images were captured at the same field of view at 4-second intervals. The end-to-end distance (R) was measured for selected worm micelles from all the 5 frames and contour length (L) of the worm micelle was measured from at least two fully extended conformations of the selected worm micelle. This was repeated for 10 different worm micelles spanning in contour length (L) between 4 μm to 15 μm. The persistence length (l_p) was estimated by fitting the data to a worm-like chain model defined by $\langle R^2 \rangle = 2(lp)^2[(L/l_p)-1+\exp(-L/l_p)]$. The effect of dye concentration on the worm micelle flexibility was studied by adding 2 μL of 0.02 mM dye (PKH26, Sigma) to samples prepared at three different concentrations; 1000 μM, 100 μM and 10 μM (S10).

Contour length distribution of worm micelles

100 μL of 100 μM labeled worm micelle solution was taken in an Eppendorf tube and 0.2 μL of dye (0.2 mM PKH26, Sigma) was added and the contents were diluted to 400 μL with DI water. Prior to imaging, 10 μL of 100 mM NaCl solution was added and mixed gently. From this 3 μL was taken on a glass slide and 25×25 mm square cover-slip was placed on top and pressed hard and sealed on the sides vacuum grease. The addition of salt permits sticking of the labeled worm micelles to the glass surface. The cover slip was imaged using 60× lens with oil at 1.5× magnification on a Olympus IX71 microscope equipped with a Cascade 512B camera. If necessary the worm micelle solution was further diluted during sample preparation so that worm micelles do not touch each other in the images and salt concentration was adjusted so that all the worm micelles were immobilized on glass surface. For each sample, 20 frames were imaged and the worm length was measured using Matlab program (S8). A custom Matlab code, using elongated Laplacian of Gaussian filters to detect line-like structures was used to automatically segment the fluorescent images of worm micelles. From this contour lengths were computed for close to 1000 worms. Detailed procedure is described in S13.

Phase contrast imaging of OCL (2, 13.5) vesicles

To the dried vial containing a thin film of OCL(2,13.5) polymer, 1 mL of 300 mOsm sucrose was added and placed in a pre-heated oven at 60°C with cap closed for 12 hrs under gentle stirring (~100 rpm). For imaging, 10 μL of sample was placed within a thin chamber prepared between a glass slide and cover slip using vacuum grease.

Micropipette aspiration of OCL (2, 13.5) and OB (3.5, 6.75) vesicles

Micropipette aspiration studies were performed as previously described using Narishige manipulators (Tokyo) that was connected to a custom manometer system with pressure transducers (Validyne, Northridge, CA) for control and monitoring of the aspiration pressure.[42] Pure OCL (2, 13.5) and OB (3.5, 6.75) vesicles were prepared by film re-hydration method and labeled with a hydrophobic dye (PKH 26, Sigma). The vesicles were first immobilized by applying a nominal pressure of 10 mm of Hg and then the pressure is gradually increased. Aspirated vesicles were imaged using bright-field and epi-fluorescence on a Nikon TE-300 inverted microscope.

Supplementary Material

Refer to Web version on PubMed Central for supplementary material.

Acknowledgments

This work was supported by NSF MRSEC, NTI, and NIH-NIBIB.

References

1. Alexandridis P, Lindman B. Amphiphilic Block Copolymers: Self-Assembly and Applications. 2000:435.
2. Discher DE, Eisenberg A. Science (Washington, DC, United States). 2002; 297(5583):967–973.
3. Discher BM, Won Y-Y, Ege DS, Lee JCM, Bates FS, Discher DE, Hammer DA. Science (Washington, D. C.). 1999; 284(5417):1143–1146.
4. Dalhaimer P, Bates FS, Discher DE. Macromolecules. 2003; 36(18):6873–6877.
5. Won Y-Y, Davis HT, Bates FS. Science (Washington, D. C.). 1999; 283(5404):960–963.
6. Dalhaimer P, Bermudez H, Discher DE. Journal of Polymer Science, Part B: Polymer Physics. 2003; 42(1):168–176.
7. Kim Y, Dalhaimer P, Christian DA, Discher DE. Nanotechnology. 2005; 16(7):484–491.
8. Geng Y, Dalhaimer P, Cai S, Tsai R, Tewari M, Minko T, Discher DE. Nature Nanotechnology. 2007; 2(4):249–255.
9. Discher DE, Ortiz V, Srinivas G, Klein ML, Kim Y, Christian D, Cai S, Photos P, Ahmed F. Progress in Polymer Science. 2007; 32(8–9):838–857.
10. Kim Y, Tewari M, Pajerowski JD, Cai S, Sen S, Williams J, Sirsi S, Lutz G, Discher DE. Journal of Controlled Release. 2009; 134(2):132–140. [PubMed: 19084037]
11. Christian DA, Cai S, Bowen DM, Kim Y, Pajerowski JD, Discher DE. European Journal of Pharmaceutics and Biopharmaceutics. 2009; 71(3):463–474. [PubMed: 18977437]
12. Loo YL, Register RA, Ryan AJ. Macromolecules. 2002; 35(6):2365–2374.
13. Jain S, Bates FS. Science (Washington, DC, United States). 2003; 300(5618):460–464.
14. Israelachvili JN. Intermolecular and Surface Forces. 1991:291.
15. Kim SY, Shin IG, Lee YM, Cho CS, Sung YK. Journal of controlled release official journal of the Controlled Release Society. 1998; 51(1):13–22. [PubMed: 9685900]
16. Allen C, Yu Y, Maysinger D, Eisenberg A. Bioconjugate Chemistry. 1998; 9(5):564–572. [PubMed: 9736490]

17. Park YJ, Lee JY, Chang YS, Jeong JM, Chung JK, Lee MC, Park KB, Lee SJ. Biomaterials. 2001; 23(3):873–879. [PubMed: 11771706]
18. Montazeri Aliabadi H, Brocks DR, Lavasanifar A. Biomaterials. 2005; 26(35):7251–7259. [PubMed: 16005061]
19. Shi B, Fang C, You MX, Zhang Y, Fu S, Pei Y. Colloid and Polymer Science. 2005; 283(9):954–967.
20. Soo PL, Lovric J, Davidson P, Maysinger D, Eisenberg A. Molecular Pharmaceutics. 2005; 2(6): 519–527. [PubMed: 16323959]
21. Letchford K, Liggins R, Wasan KM, Burt H. European Journal of Pharmaceutics and Biopharmaceutics. 2009; 71(2):196–206. [PubMed: 18762253]
22. Otsuka H, Nagasaki Y, Kataoka K. Advanced Drug Delivery Reviews. 2003; 55(3):403–419. [PubMed: 12628324]
23. Champion JA, Mitragotri S. Proceedings of the National Academy of Sciences of the United States of America. 2006; 103(13):4930–4934. [PubMed: 16549762]
24. Gratton SEA, Ropp PA, Pohlhaus PD, Luft JC, Madden VJ, Napier ME, De Simone JM. Proceedings of the National Academy of Sciences of the United States of America. 2008; 105(33): 11613–11618. [PubMed: 18697944]
25. Ghoroghchian PP, Li G, Levine DH, Davis KP, Bates FS, Hammer DA, Therien MJ. Macromolecules. 2006; 39(5):1673–1675. [PubMed: 20975926]
26. Fairley N, Hoang B, Allen C. Biomacromolecules. 2008; 9(9):2283–2291. [PubMed: 18702541]
27. Du Z-X, Xu J-T, Fan Z-Q. Macromolecules (Washington, DC, United States). 2007; 40(21):7633–7637.
28. Zupancich JA, Bates FS, Hillmyer MA. Macromolecules. 2006; 39(13):4286–4288.
29. Kamber NE, Jeong W, Waymouth RM, Pratt RC, Lohmeijer BGG, Hedrick JL. Chemical Reviews (Washington, DC, United States). 2007; 107(12):5813–5840.
30. Kricheldorf HR, Bornhorst K, Hachmann-Thiessen H. Macromolecules. 2005; 38(12):5017–5024.
31. Moravek SJ, Storey RF. Journal of Macromolecular Science, Part A Pure and Applied Chemistry. 2009; 46(4):339–345.
32. Hu H, Dorset DL. Macromolecules. 1990; 23(21):4604–7.
33. Zhang L, Eisenberg A. Science (Washington, D. C.). 1995; 268(5218):1728–31.
34. Cui HG, Chen ZY, Zhong S, Wooley KL, Pochan DJ. Science. 2007; 317(5838):647–650. [PubMed: 17673657]
35. Discher BM, Bermudez H, Hammer DA, Discher DE, Won YY, Bates FS. Journal of Physical Chemistry B. 2002; 106(11):2848–2854.
36. Srinivas G, Discher DE, Klein ML. Nature Materials. 2004; 3(9):638–644.
37. Rubinstein, MC.; Ralph. Polymer Physics. Oxford University Press Inc.; New York: 2003.
38. Rawicz W, Olbrich K, McIntosh T, Needham D, Evans E. Biophysical Journal. 2000; 79(1):328–339. [PubMed: 10866959]
39. Wang X, Guerin G, Wang H, Wang Y, Manners I, Winnik MA. Science (Washington, DC, United States). 2007; 317(5838):644–647.
40. Blicher A, Wodzinska K, Fidorra M, Winterhalter M, Heimburg T. Biophysical Journal. 2009; 96(11):4581–4591. [PubMed: 19486680]
41. Seung HS, Nelson DR. Physical Review A. 1988; 38(2):1005–1018. [PubMed: 9900464]
42. Bermudez H, Brannan AK, Hammer DA, Bates FS, Discher DE. Macromolecules. 2002; 35(21): 8203–8208.

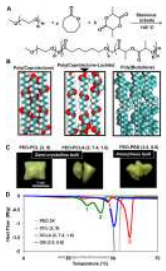

Scheme 1.

Synthesis and bulk phase characterization of polymers. **A** Synthesis of polyethyleneoxide-*b*-poly(caprolactone-*random*-DL-lactide) block copolymer (OCLA). **B** Panels from left to right show the space filling models of polycaprolactone, poly(caprolactone-*r*-DL-lactide), and 1,4 polybutadiene blocks. The presence of *DL*-lactide affects molecular level packing and possibly limits the extent of crystallization. **C** Images of the physical state of bulk OCL(2, 9), OCLA (2, 7.4, 1.6) and OB (3.5, 6.8) block copolymers. **D** Differential scanning calorimetry scans of PEO, OCL(2, 9), OCLA(2, 7.4, 1.6) and OB (3.5, 6.8) block copolymers in solid state.

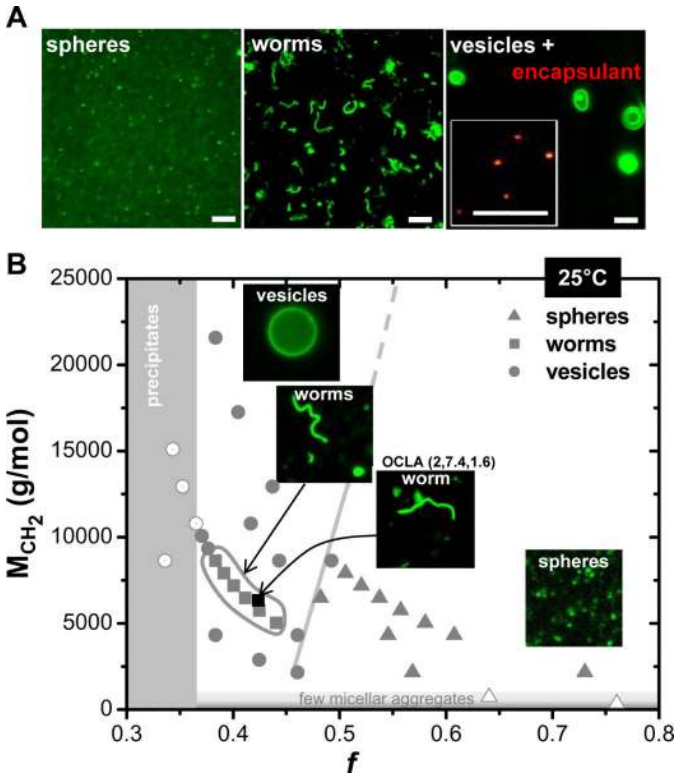

Figure 1.

Morphological phase behavior of OCL polymers in dilute solution. **A** Representative fluorescent micrographs of spherical micelles, worm micelles and vesicles imaged after lebeling with a lipophilic dye is shown. Inset in the panel on far right shows localization of FITC-dextran (4000g/mole) within sub-micron sized OCL vesicles. **B** Morphological phase behavior of OCL assemblies in dilute solution prepared at 25°C by chloroform evaporation method. Filled symbols in grey represent corresponding morphologies; triangles for spherical micelles, squares for worm micelles and circles for vesicles. Grey lines indicate the approximate phase boundaries. Worm micelles formed from OCLA (2, 7.4, 1.6) copolymer is indicated in the phase diagram with a filled black square. Scale bar is 10 μm.

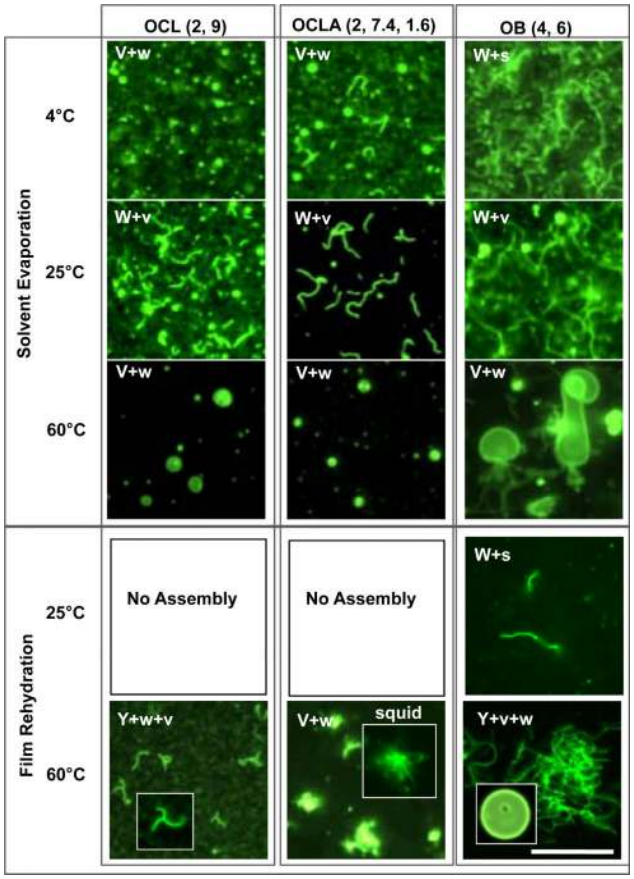

Figure 2.

Temperature and process dependence of morphologies. Morphologies of OCL(2, 9), OCLA(2, 7.4, 1.6) and OB(4, 6) polymers formed by solvent evaporation and film rehydration methods at different temperatures is shown. At 4°C no significant self-assembly was observed by film rehydration method for OCL and OCLA polymers after two weeks. The morphologies obtained is indicated by letter codes on the top left of each panel: S for spherical micelles, W for wormlike micelles, V for vesicles and Y for Y-junctions. The first letter refers to the dominant morphology observed. Scale bar is 10 μm.

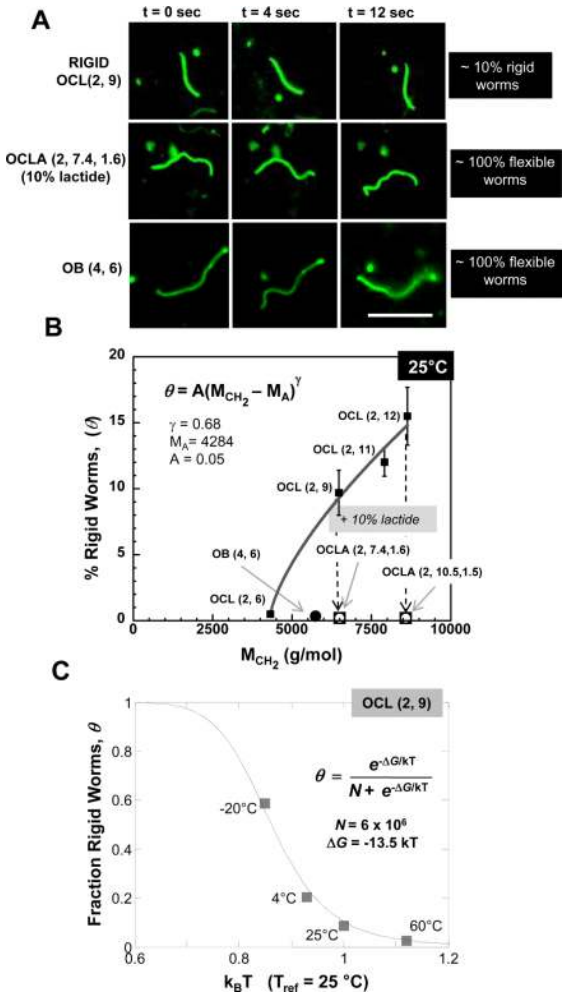

Figure 3.

Controlling rigidity of worm micelles. **A** Fluorescence microscopy snap shots representing worm micelle conformation at 4 sec intervals is shown for a rigid OCL(2, 9) worm micelle (top row), a flexible OCLA(2, 7.4, 1.6) worm micelle (middle row) and a flexible OB(4,6) worm micelle (bottom row). Approximately 10% of OCL(2, 9) worm micelles exhibit rigid-body motion at room temperature while all of OCLA and OB worm micelles are completely flexible. Scale bar for all images is 10 μm. **B** Percentage of rigid OCL worm micelles (θ) as a function of the size of the hydrophobic block (M_{CH2}) is shown. The data is fit to a power law ($R^2 = 0.985$). The absence of rigid worm micelles in OB and OCLA samples is also indicated. **C** The fraction of rigid OCL(2, 9) worm micelles (θ) as a function of temperature in k_BT units is shown. See text for fit.

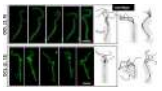

Figure 4.
Visualization of partial rigidity in OCL worm micelles. Snapshots were taken every 30 sec of OCL worms, and the contour was traced, rotated, and overlaid to highlight the rigid segment. Scale bar is 5 μm.

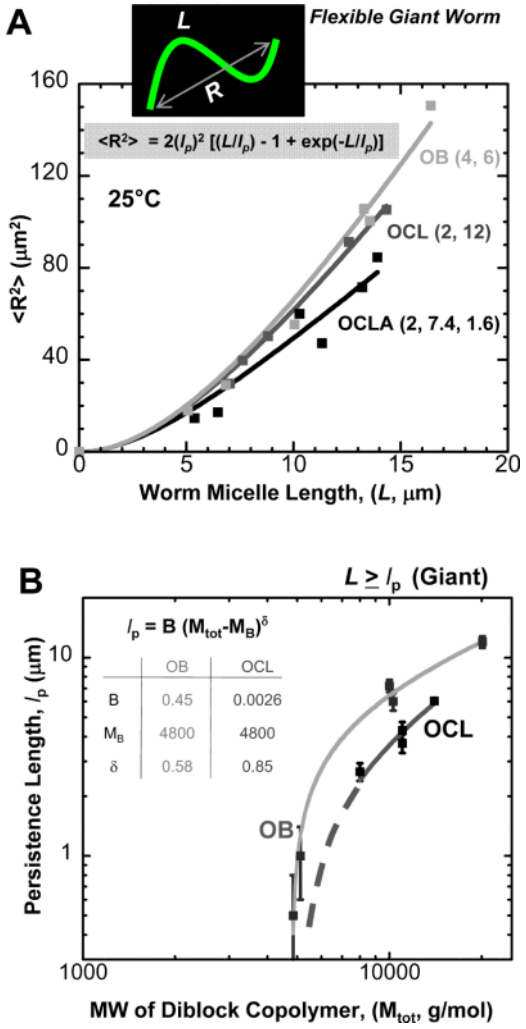

Figure 5.

Flexibility of OCL and OCLA worm micelles. **A** The mean square end-to-end distance $\langle R^2 \rangle$ is plotted against the contour length *L* for OCL(2, 12), OCLA(2, 7.4, 1.6) and OB(4, 6) worm micelles. R and *L* were measured from the time-lapse fluorescence microscopy images of worm micelles imaged at 4 second intervals. **B** The scaling of worm micelle persistence length as a function of the total molecular weight (M_{tot}) is shown for OB and OCL diblock copolymers. See text for fit.

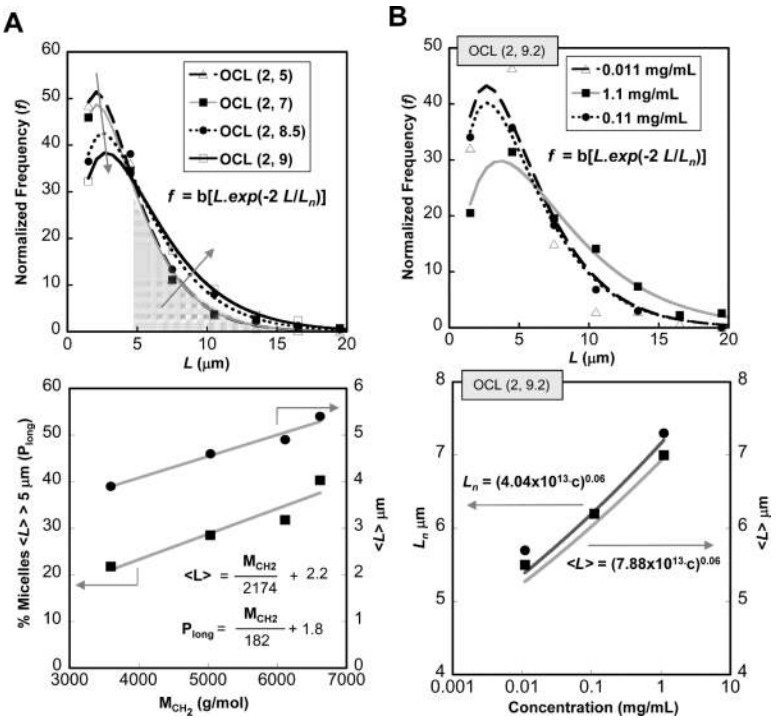

Figure 6.

Contour lengths of worm micelles. **A** The distribution of contour length is shown for four worm micelle forming OCL polymers: OCL(2,5)(Δ), OCL(2, 7)(■),OCL(2, 8.5)(●),OCL(2, 9.2)(□). The distribution data is fit to a Zimm-Shulz model. All fits shown had $R^2 > 0.99$. Arrows indicate the change in contour length distribution as the size of polycaprolactone block (M_{CH2}) is increased. The bottom panel shows the population of worm micelles longer than 5 μm (P_{long}, left axis) and experimentally determined average contour length $\langle L \rangle$ (right axis) as a function of the size of the hydrophobic block (M_{CH2}). The fits for P_{long} ($R^2 = 0.98$) and $\langle L \rangle$ ($R^2 = 0.96$) are shown to scale linearly with M_{CH2}. **B** The concentration dependence of worm micelle length is shown for OCL (2, 9.2) polymer at three different concentrations (c). The data is fit to a Zimm-Shulz model. All fits shown had $R^2 > 0.97$. Arrows indicate the change in contour length distribution as the concentration (c) of the polymer is increased. The bottom panel shows the number average contour length (L_n, left axis) and the experimentally determined average contour length ($\langle L \rangle$, right axis) for OCL (2, 9.2) sample. The fits for L_n ($R^2 = 0.97$) and $\langle L \rangle$ ($R^2 = 0.96$) are shown to scale with c.

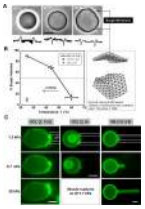

Figure 7.

Rigidity of OCL membranes. **A** Representative phase contrast image of OCL (2, 13.5) vesicle imaged after equilibrating at 60°C, 43°C and 25°C. The vesicles were prepared by film rehydration at 60°C in 300 mOsm sucrose and diluted in 300 mOsm glucose before equilibration. The retention of sucrose within vesicle at 60°C is evident from the phase dark image shown in left panel. Image of crystalline membrane roughened by a dislocation defect is from Seung and Nelson (1998). **B** Proportion of OCL(2, 13.5) vesicles that are empty is shown as a function of temperature. The roughness of a solid membrane is in part due to packing disorder and disclinations that are likely to be points of distinct permeability. **C** Fluorescence microscopy images showing micropipette aspiration of OCL(2, 13.5), OCL(2, 6) and OB(3.5, 6.8) membranes at room temperature. Rigidity of OCL (2, 13.5) and OCL (2, 6) membranes is due to crystallization within the cores. While most OCL (2, 13.5) membranes do not exhibit any deformation even at high suction pressures, OCL (2, 6) membranes could not sustain high pressures. The fluidity of OB (3.5, 6.8) vesicle is evident in large deformation observed even at nominal pressures. Scale bar in all images is 10 μm.

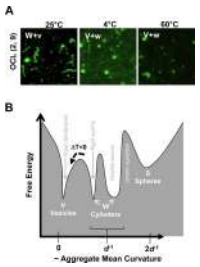

Figure 8.

Thermal stability and rugged energy landscape of OCL worm former. **A** Fluorescent micrographs of OCL(2, 9) assemblies after equilibrating at various temperatures for a day. **B** Thermodynamic representation of morphologies obtained from OCL diblock copolymers that predominantly form worm micelles. The coexistence of cylinders and vesicles is represented by similar magnitude of free energies and width of the valley represents thermally driven flexibilities in shape. The broken arrow indicates the effect of cooling on flexible worm micelles, as a result of which vesicles are formed and trapped in crystalline state.

Table 1

Molecular details of the 35 block copolymers studied

Block Copolymers	PEO (kg/mol)	PCL or PLA (kg/mol)
OCL (X, Y) *33 polymers*	X = 1	Y = 0.5, 1, 3, 4, 6, 12
	X = 2	Y = 3, 6, 7, 8, 9, 10, 11, 12, 13.5, 15, 18, 21
	X = 3.5	Y = 4, 9, 12, 15
	X = 5	Y = 3, 6, 7, 8, 9, 10, 11, 12, 18, 24, 30
OCLA (X, Y, Z)	X = 2	Y = 7.4 and Z = 1.6 Y = 10.5 and Z = 1.5